Acta Crystallographica Section F
Structural Biology and Crystallization Communications
ISSN 1744-3091

The ParE2–PaaA2 toxin–antitoxin complex from *Escherichia coli* O157 forms a heterodocecamer in solution and in the crystal

Yann G. J. Sterckx,[a,b] Abel Garcia-Pino,[a,b] Sarah Haesaerts,[a,b] Thomas Jové,[c] Lieselotte Geerts,[a] Viktor Sakellaris,[a] Laurence Van Melderen[c] and Remy Loris[a,b]*

[a]Structural Biology Brussels, Department of Biotechnology, Vrije Universiteit Brussel, Pleinlaan 2, B-1050 Brussel, Belgium, [b]Molecular Recognition Unit, Department of Structural Biology, VIB, Pleinlaan 2, B-1050 Brussel, Belgium, and [c]Génétique et Physiologie Bactérienne, Université Libre de Bruxelles, 12 Rue des Professeurs Geener et Brachet, B-6041 Gosselies, Belgium

Correspondence e-mail: remy.loris@vib-vub.be

Received 7 March 2012
Accepted 6 April 2012

Escherichia coli O157 *paaR2-paaA2-parE2* constitutes a unique three-component toxin–antitoxin (TA) module encoding a toxin (ParE2) related to the classic *parDE* family but with an unrelated antitoxin called PaaA2. The complex between PaaA2 and ParE2 was purified and characterized by analytical gel filtration, dynamic light scattering and small-angle X-ray scattering. It consists of a particle with a radius of gyration of 3.95 nm and is likely to form a heterododecamer. Crystals of the ParE2–PaaA2 complex diffract to 3.8 Å resolution and belong to space group $P3_121$ or $P3_221$, with unit-cell parameters $a = b = 142.9$, $c = 87.5$ Å. The asymmetric unit is consistent with a particle of around 125 kDa, which is compatible with the solution data. Therefore, the ParE2–PaaA2 complex is the largest toxin–antitoxin complex identified to date and its quaternary arrangement is likely to be of biological significance.

1. Introduction

Bacteria need their internal physiology to be in tune with the external environment and to respond to changes in the availability of nutrients, the growth temperature, toxic substances such as antibiotics and/or bacteriocins and other types of stresses. Among the arsenal of macromolecules that are available to function in the context of bacterial stress response are the so-called 'toxin–antitoxin (TA)' modules. These are pairs of genes, usually forming a separate small operon, that were originally discovered to be involved in the maintenance of low-copy-number plasmids (Ogura & Hiraga, 1983; Gerdes *et al.*, 1986; Bravo *et al.*, 1987; Lehnherr *et al.*, 1993). They are now known to be abundant on bacterial chromosomes, with some organisms such as *Mycobacterium tuberculosis* possessing over 60 TA modules (Pandey & Gerdes, 2005). Various roles have been attributed to TA modules, including selfish entities and the stabilization of labile chromosomal segments (Magnuson, 2007; Van Melderen, 2010). Most researchers nevertheless agree on an involvement in stress response, given that various internal and external stresses lead to their activation (Christensen *et al.*, 2001; Amitai *et al.*, 2009; Kolodkin-Gal *et al.*, 2009) and that at least in some cases differential activation is observed based on the type of stress encountered (Fiebig *et al.*, 2010). However, since knocking out of individual TA modules does not seem to affect bacterial survival upon stress exposure in most bacteria, this may be a secondary effect (Tsilibaris *et al.*, 2007). However, TA systems have been shown to be essential to cell survival in *M. smegmatis* (Frampton *et al.*, 2012). Most interesting is the recent discovery that all TA modules on the *Escherichia coli* chromosome contribute in a cumulative manner to the fraction of persisters in the population (Maisonneuve *et al.*, 2011). Direct involvement in persistence could explain both their activation during stress episodes and why an organism such as *M. tuberculosis* displays such a high degree of persistence.

Many different families of TA modules exist, encoding toxins with distinct modes of action and antitoxins with different types of DNA-

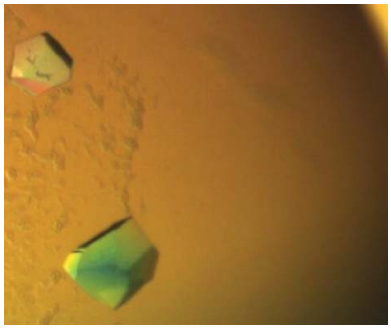

binding domain (Gerdes *et al.*, 2005; Buts *et al.*, 2005; Yamaguchi & Inouye, 2009; Hayes & Van Melderen, 2011). While initially it was thought that each family of toxins was associated with a particular family of antitoxin, recent genomic surveys have indicated that almost any toxin–antitoxin combination is possible (Leplae *et al.*, 2011). The antitoxin is a modular protein with a DNA-binding domain of variable fold linked to a (usually) intrinsically disordered toxin-neutralizing segment. This toxin-neutralizing segment binds to or even complements the fold of the toxin and inhibits its biochemical activity (Kamada *et al.*, 2003; Kamada & Hanaoka, 2005; Garcia-Pino *et al.*, 2008; Li *et al.*, 2009; De Jonge *et al.*, 2009; Brown *et al.*, 2009). This activity depends on the family of toxin considered and may include poisoning DNA gyrase (Bernard & Couturier, 1992; Jiang *et al.*, 2002), cleaving RNA in a ribosome-dependent or independent fashion (Zhang *et al.*, 2003; Christensen-Dalsgaard & Gerdes, 2008; Zhang & Inouye, 2011), direct ribosome inhibition (Liu *et al.*, 2008), chemical modification of ribosomes (Vesper *et al.*, 2011), modifying initiator tRNA (Winther & Gerdes, 2011) or a number of other activities that directly alter the basic physiology of the cell (Yamamoto *et al.*, 2009; Tan *et al.*, 2010; Mutschler *et al.*, 2011).

The *parDE* family of TA modules encodes a toxin (ParE) that poisons gyrase and thus interferes with transcription and replication (Jiang *et al.*, 2002). While not as well characterized in terms of mechanism and structure as the CcdB proteins (Dao-Thi *et al.*, 2005; De Jonge *et al.*, 2009), recent data indicate that the binding site on gyrase for the two types of toxins is different (Yuan *et al.*, 2010). In the classic *parDE* modules ParE is neutralized by the antitoxin ParD, which consists of an N-terminal ribbon–helix–helix (RHH) DNA-binding domain involved in auto-repression and a relatively long C-terminal domain (45 and 50 amino acids for ParE from *E. coli* plasmid RK2 and from *Caulobacter crescentus*, respectively) that is intrinsically disordered in its native state (Oberer *et al.*, 2007). Upon binding to ParE, the C-terminal domain mainly folds into large helical segments that wrap around ParE (Dalton & Crosson, 2010).

Recently, two three-component ParE-containing TA operons have been identified on the chromosome of *E. coli* O157 (Hallez *et al.*, 2010). These operons contain a ParE homologue downstream of a transcription regulator of the DicA transcriptional repressor family (PaaR) and an antitoxin (PaaA) which is shorter than the classic ParD antitoxins and does not display any significant sequence identity to known ParD proteins. Interestingly, regulation of the system requires all three components (Hallez *et al.*, 2010). In this paper, we describe the overexpression, purification, preliminary characterization and crystallization of the ParE2–PaaA2 complex encoded by the *paaR2-paaA2-parE2* operon on the chromosome of *E. coli* O157.

2. Materials and methods

2.1. Cloning, protein production and purification

The *paaA2-parE2* coding region (UniProtKB accession Nos. NP_288008 and NP_310308) was picked up out of *E. coli* O157:H7 EDL933 as described by Hallez *et al.* (2010) and was introduced into the pET21b vector (Novagen) *via* the *Eco*RI and *Xho*I sites using the primers 5′-GAATTCAGGAGGGAGTAATGGATTATAAAGATG-ACGATGACAAAAATAGAGCCCTTTCACCA-3′ (forward) and 5′-CGCAAGACGCCAGTTTCCCCTCGAG-3′ (reverse). This provides PaaA2 with an N-terminal FLAG tag (DYKDDDDK) and ParE2 with a C-terminal His tag (LEHHHHHH) attached to their native sequences.

pET21b-*paaA2-parE2* was transformed in *E. coli* strain BL21 (DE3) (Studier *et al.*, 1990) using the $CaCl_2$ method (Hanahan *et al.*, 1991). Transformed cells were selected on LB plates containing ampicillin (100 µg ml^{-1}) and 2%(*w*/*v*) glucose and were grown overnight at 310 K. An individual colony was picked to start an overnight 100 ml pre-culture incubated in Luria–Bertani medium (Bertani, 1951) containing 100 µg ml^{-1} ampicillin and 0.2%(*w*/*v*) glucose at 310 K with aeration. A 10 l culture was then started by inoculating ten bottles containing 1 l LB medium supplemented with 100 µg ml^{-1} ampicillin and 0.2%(*w*/*v*) glucose with a 100-fold dilution of the pre-culture. Induction of gene expression was obtained by the addition of 1 m*M* IPTG when an OD_{600} of 0.6 had been reached. Cultures were grown overnight at 310 K with aeration and harvested by centrifugation for 20 min [6500*g* (5000 rev min^{-1} in a JLA-8.1000 rotor), 277 K]. The bacterial pellets were resuspended in lysis buffer (50 m*M* Tris–HCl pH 8.0, 500 m*M* NaCl, 20 m*M* imidazole, 0.1 mg ml^{-1} AEBSF, 1 µg ml^{-1} leupeptin, 1 m*M* EDTA) and aliquoted in volumes of 50 ml. The aliquots were flash-cooled using liquid nitrogen and stored at 192 K.

Cells were lysed using a French press or a cell disruptor and the cell lysate was centrifuged for 20 min [29 000*g* (15 000 rev min^{-1} in a JA-20 rotor), 277 K]. The soluble fraction was kept aside and filtered (0.45 µm) prior to purification. The ParE2–PaaA2 complex was purified on an ÄKTAexplorer platform (GE Healthcare) using immobilized metal-affinity chromatography (IMAC; Porath *et al.*, 1975) and size-exclusion chromatography (SEC). A 1 ml HisTrap HP Nickel Sepharose column (GE Healthcare) was equilibrated with washing buffer (50 m*M* Tris–HCl pH 8.0, 500 m*M* NaCl, 20 m*M* imidazole) for at least five column volumes. The sample was loaded onto the column using the washing buffer. The ParE2–PaaA2 complex was eluted by gradually increasing the imidazole concentration present in the elution buffer (50 m*M* Tris–HCl pH 8.0, 500 m*M* NaCl, 1 *M* imidazole) from 0 to 100% over 20 column volumes. The fractions containing ParE2–PaaA2 were pooled and concentrated (Amicon Ultra UltraCel 3K) for subsequent SEC. A Superdex 200 16/60 column (GE Healthcare) was pre-equilibrated for at least one column volume using SEC buffer (50 m*M* Tris–HCl pH 8.0, 500 m*M* NaCl) and run at 1.0 ml min^{-1}. Fractions containing ParE2–PaaA2 were pooled, flash-cooled using liquid nitrogen and stored at 193 K. The progress of the purification was monitored by SDS–PAGE (Laemmli, 1970) and Western blotting (Towbin *et al.*, 1979). For concentration determination, a 1:1 stoichiometry was assumed for the ParE2–PaaA2 complex, leading to a calculated extinction coefficient of 1.34 mg^{-1} ml cm^{-1} for a species of 20.2 kDa including the affinity tags.

2.2. Crystallization

Protein samples were dialyzed against a suitable buffer (20 m*M* Tris–HCl pH 8.0, 100 m*M* NaCl) and concentrated to 5–20 mg ml^{-1} (Amicon Ultra UltraCel 3K). Crystallization conditions were screened manually using the hanging-drop vapour-diffusion method in 48-well plates (Hampton VDX greased) with drops consisting of 2 µl protein solution (7 mg ml^{-1}) and 2 µl reservoir solution equilibrated against 125 µl reservoir solution. Commercial screens from Hampton Research (Crystal Screen and Crystal Screen 2) and Molecular Dimensions (Morpheus) were used for screening (a total of 192 conditions were tried). The FLAG and His tags were retained on the proteins for crystallization.

The precipitant concentration, protein concentration and pH of the single promising hit [Crystal Screen condition No. 1: 20 m*M* $CaCl_2$ dihydrate, 100 m*M* sodium acetate trihydrate, 30%(*v*/*v*) (±)-2-methyl-2,4-pentanediol] were varied in an attempt to further optimize this condition. These optimizations were also performed manually using

the same 48-well plates and volumes as described above. Furthermore, microseeding was used to reduce nucleation and grow larger crystals. For the latter, five single crystals (typical dimensions 50 × 50 × 50 µm) were typically transferred to 50 µl mother liquor [20 m*M* $CaCl_2$ dihydrate, 100 m*M* sodium acetate trihydrate, 30%(*v*/*v*) (±)-2-methyl-2,4-pentanediol] and vortexed (15 s) to obtain microseeds, which were used immediately. Serial dilutions of the seeds ranging from 1 to 10^{-7} were mixed in a 1:1 ratio (2 µl each) with fresh protein solution at 7 mg ml^{-1} and equilibrated against the mother liquor. Diffraction-quality crystals typically grew after approximately 5 d at 293 K. This led to significantly larger crystals of up to 300 µm in all three dimensions.

2.3. Data collection and analysis

ParE2–PaaA2 crystals were cryoprotected either by direct transfer of the crystals into a nitrogen-gas cryostream or by first vitrifying them in liquid nitrogen without the need for an additional cryoprotectant. Crystals were screened on the PROXIMA1 beamline at the SOLEIL synchrotron (Gif-Sur-Yvette, France) during two sessions. In the first session an ADSC Q315 CCD detector was used, while the second session made use of a Pilatus 6M detector. For the final data collection, 147.2° of data were collected from a single crystal in 0.2° slices using the Pilatus detector with an exposure time of 2 s deg^{-1} and a wavelength of 0.984 Å. Data were indexed, integrated and scaled with *XDS* (Kabsch, 2010). Analysis of the unit-cell contents was performed with the program *MATTHEWS_COEF*, which is part of the *CCP*4 package (Winn *et al.*, 2011).

2.4. Biophysical characterization

Analytical gel-filtration experiments were performed on an ÄKTAexplorer platform (GE Healthcare) using a Superdex 200 HR 10/30 column (GE Healthcare) to determine the size and molecular mass of the purified ParE2–PaaA2 complex. The column was pre-equilibrated using running buffer (50 m*M* Tris–HCl pH 8.0, 500 m*M* NaCl) for at least one column volume. A 500 µl sample at a concentration of 2 mg ml^{-1} was injected using running buffer with a flow rate of 0.5 ml min^{-1}. To determine the molecular weights and the hydrodynamic radii of the proteins (Uversky, 1993), the column was calibrated using molecular-weight standards from Bio-Rad.

Dynamic light-scattering (DLS) experiments were performed on a DynaPro (Protein Solutions) plate reader (Wyatt Technology) in 50 m*M* Tris–HCl pH 8.0, 500 m*M* NaCl at room temperature (293 K). Data were measured for ParE2–PaaA2 samples at different concentrations (1–10 mg ml^{-1}).

Small-angle X-ray scattering (SAXS) studies were conducted on the SWING beamline at the SOLEIL synchrotron, Gif-sur-Yvette, France in HPLC mode (David & Pérez, 2009). A total volume of 80 µl ParE2–PaaA2 sample at 10 mg ml^{-1} was injected onto a Shodex KW404-4F column (Shodex) which had been pre-equilibrated with running buffer (50 m*M* Tris–HCl pH 7.5, 500 m*M* NaCl) for at least one column volume. The flow rate was set to 0.25 ml min^{-1} and data were collected with an exposure time of 0.5 s and a dead time of 1.0 s. Buffer data were collected at the beginning of the chromatogram and sample data were collected in the peak area. Data processing and analysis was performed with the programs provided in the *ATSAS* package (Konarev *et al.*, 2006) and the online *SAXS MoW* application (Fischer *et al.*, 2010).

3. Results and discussion

The coding region of the *paaA2* and *parE2* genes of *E. coli* O157 was inserted into plasmid pET21b and introduced into *E. coli* BL21 (DE3) in order to obtain an expression clone that produces an N-terminally FLAG-tagged version of PaaA2 and a C-terminally His-tagged version of ParE2. Optimal conditions for protein production were obtained by varying the density of the culture before induction and the time of harvest after induction with 1 m*M* IPTG. Assuming equimolar production of proteins ($\varepsilon_{280\ nm}$ = 1.34 mg^{-1} ml cm^{-1} for a ParE2–PaaA2 homodimer), about 50 mg protein is produced per litre of culture after overnight induction. IMAC purification resulted in a single peak that eluted at around 0.2 *M* imidazole and contained both PaaA2 and ParE2. During a subsequent gel-filtration step to remove remaining contaminants, both proteins co-eluted in a single peak, indicating the existence of a distinct ParE2–PaaA2 antitoxin–toxin complex.

Analytical gel filtration indicates that this complex has a molecular mass of around 140 kDa (Fig. 1*a*), which is unexpectedly large given the low molecular weights of the constituents of the toxin–antitoxin complex (8.5 kDa for PaaA2 and 11.7 kDa for ParE2 including their affinity tags). The DLS experiments (Fig. 1*b*) at a concentration of 10 mg ml^{-1} support these findings as they indicate the presence of a single type of particle with a hydrodynamic radius (R_h) of 4.81 nm and a molecular weight of 133 kDa, which are fully consistent with

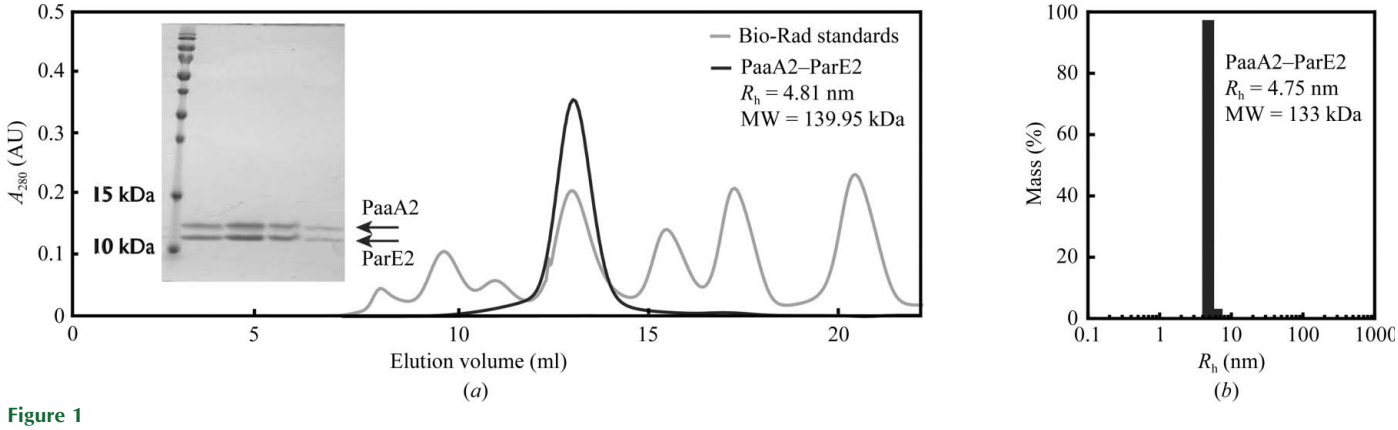

Figure 1
Characterization of the hydrodynamic properties of the ParE2–PaaA2 complex. (*a*) Analytical gel filtration shows that the ParE2–PaaA2 complex elutes as a single peak at 13.05 ml, corresponding to a molecular weight of 140 kDa and a hydrodynamic radius of 4.81 nm. The inset shows an SDS–PAGE (15% gel) analysis of the elution peak, which clearly demonstrates that both PaaA2 and ParE2 are present in the complex. (*b*) DLS measurements performed under the same conditions as the analytical gel-filtration experiment confirm that the ParE2–PaaA2 preparations contain a single particle with (within error limits) identical hydrodynamic properties.

the values for the molecular weight and R_h calculated based on the analytical gel-filtration data. Furthermore, analytical SEC and DLS experiments performed at lower concentrations (up to 1 mg ml^{-1}) yield the same result, indicating that the formation of a large oligomer by PaaA2 and ParE2 is not concentration-dependent (data not shown).

The unanticipated large size of the ParE2–PaaA2 complex (compared with other TA complexes and given the size of the individual proteins) was further confirmed by small-angle X-ray scattering (SAXS). These measurements confirm that the ParE2–PaaA2 complex is a large single species with a radius of gyration of 3.95 nm and an estimated molecular weight of around 160 kDa (Fig. 2). Comparison of the radius of gyration R_g and the hydrodynamic radius R_h suggests that the particle is globular. For a solid sphere, the ratio between its radius of gyration and hydrodynamic radius is about 0.775; based on the presented findings, this ratio is 0.823 for the ParE2–PaaA2 complex. This suggests that the formed complex is relatively compact. This is further advocated by the Kratky plot, which indicates that the complex is indeed a well folded entity without significant disordered regions (Fig. 2, inset).

Screening of crystallization conditions led to a single hit in 20 m*M* $CaCl_2$ dihydrate, 100 m*M* sodium acetate trihydrate, 30%(*v*/*v*) (±)-2-methyl-2,4-pentanediol (Crystal Screen condition No. 1; Fig. 3*a*). Varying the protein concentration, pH and precipitant concentration did not lead to any further optimization. Larger crystals could nevertheless be obtained through microseeding (Fig. 3*b*; see §2 for details). The presence of both ParE2 and PaaA2 in the crystals was confirmed by washing a few crystals in artificial mother liquor, dissolving them in water and analyzing them by SDS–PAGE (Fig. 3*c*).

Crystals mounted at room temperature (293 K) in MiTeGen MicroRT X-ray capillaries did not show any crystalline diffraction. When vitrified directly in the cold stream, weak crystalline diffraction was observed which at best extended to 6 Å resolution. Attempts at annealing or controlled dehydration systematically resulted in a complete loss of diffraction power and physical damage to the crystal in the form of extensive cracking. When vitrified in liquid nitrogen, the crystals showed significantly improved diffraction, although with variable quality. Most crystals treated this way diffract to between 5 and 4 Å resolution. However, diffraction is occasionally observed to 3.8 Å resolution (Fig. 3*d*). The resulting data-collection statistics for the best crystal (dimensions 300 × 250 × 250 µm) among about 100 crystals that were tested are given in Table 1. The crystals belong to space group $P3_121$ or $P3_221$, with unit-cell parameters $a = b = 142.9$, $c = 87.5$ Å. Matthews analysis suggests that the asymmetric unit is compatible with 4–6 ParE2–PaaA2 heterodimers (Table 2). In the light of our solution studies, it is most likely that the asymmetric unit consists of a single heterododecameric particle with a molecular weight of 123.6 kDa, although the exact stoichiometry of this complex and its arrangement should be subjected to further research.

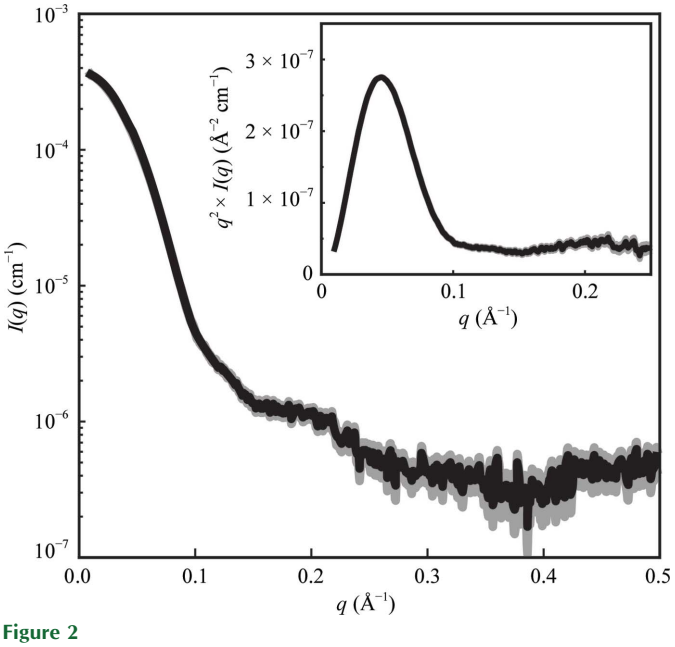

Figure 2
Small-angle X-ray scattering experiments. The experimental data are shown in black, while the error margins are shown in grey. Analysis of the scattering curve indicates that the ParE2–PaaA2 complex is a unique globular entity with a radius of gyration of 3.95 nm [determined through Guinier and $P(r)$ analysis] and a molecular weight of about 140–160 kDa (determined through Guinier, Porod and *SAXS MoW* analyses). The inset shows the Kratky plot.

Table 1
Data-collection statistics.

Values in parentheses are for the highest resolution shell.

Beamline	PROXIMA1, SOLEIL
Resolution range (Å)	46.8–3.8 (4.0–3.8)
Unit-cell parameters (Å, °)	$a = b = 142.9$, $c = 87.5$, $\alpha = \beta = 90$, $\gamma = 120$
Space group	$P3_121$ or $P3_221$
Mosaicity (°)	0.30
R_{merge}†	0.094 (0.540)
No. of measured reflections	82058 (11512)
No. of unique reflections	10405 (1559)
Multiplicity	7.9 (7.4)
$\langle I/\sigma(I)\rangle$	12.4 (2.9)
Completeness (%)	97.5 (92.8)

† $R_{merge} = \sum_{hkl}\sum_i |I_i(hkl) - \langle I(hkl)\rangle| / \sum_{hkl}\sum_i I_i(hkl)$.

Table 2
Matthews analysis assuming a 1:1 stoichiometry between ParE2 and PaaA2.

No. of ParE2–PaaA2 heterodimers in asymmetric unit	V_M (Å^3 Da^{-1})	Solvent content (%)	Probability
2	6.42	80.86	0.00
3	4.28	71.28	0.01
4	3.21	61.71	0.11
5	2.57	52.14	0.41
6	2.14	42.57	0.41
7	1.83	33.00	0.04
8	1.61	23.42	0.00

Although the details of the structure of the ParE2–PaaA2 complex will need to await structure determination by isomorphous replacement or anomalous scattering, it is clear that this complex is unexpectedly large for two small proteins. A number of other toxin–antitoxin pairs (*e.g.* CcdAB, Kis–Kid and Phd–Doc) have also been shown to form larger aggregates under certain conditions, but in these cases nonglobular chains of variable length consisting of alternating toxin and antitoxin molecules were identified (Dao-Thi *et al.*, 2002; Kamphuis *et al.*, 2007; Garcia-Pino *et al.*, 2010). These extended structures have recently been interpreted in terms of a specific mechanism of transcription regulation called 'conditional cooperativity' (De Jonge *et al.*, 2009; Garcia-Pino *et al.*, 2010). This type of gene regulation has recently also been demonstrated for *vapBC* TA modules, in which the toxin–antitoxin complex displays a distinct molecular architecture (Winther & Gerdes, 2012). Unlike the CcdAB and Phd–Doc TA systems, the proteins encoded by *vapBC* modules seem to assemble into a unique globular heterooctameric complex, as has been shown for VapBC from *Shigella flexneri* and *Rickettsia felis* (Dienemann *et al.*, 2011; Maté *et al.*, 2012). In both cases, these

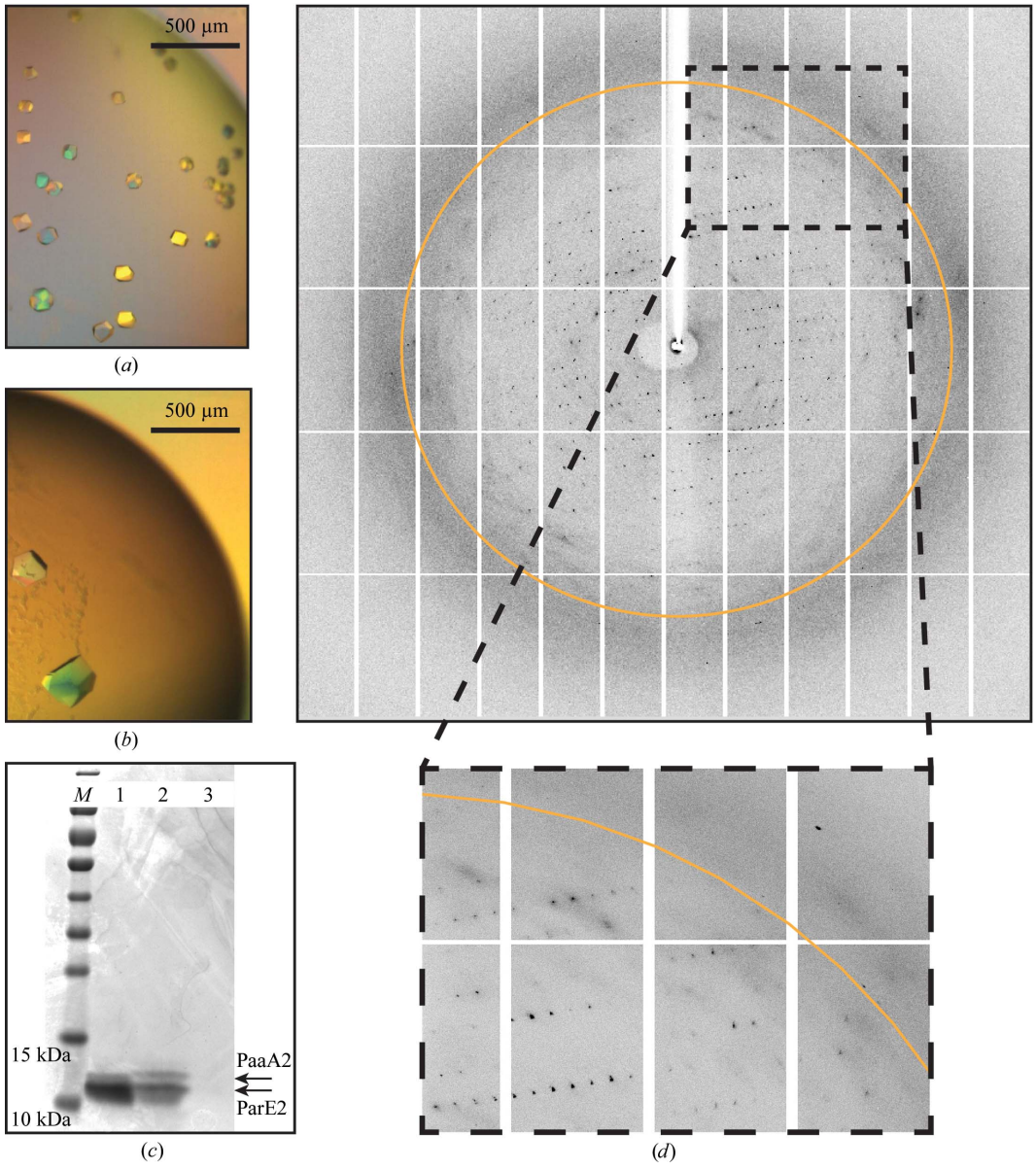

Figure 3
X-ray crystallography. (*a*) Crystals from the initial hit for the *E. coli* O157 ParE2–PaaA2 complex similar in size to those used for microseeding. The black bar indicates the size of the crystals and corresponds to 500 µm. (*b*) Typical crystals of the *E. coli* O157 ParE2–PaaA2 complex prepared by microseeding and pictured on the same scale as in (*a*). (*c*) SDS–PAGE analysis of crystals of the *E. coli* O157 ParE2–PaaA2 complex. Lane *M*, Pre-stained Molecular Weight Marker; lane 1, sample of the purified ParE2–PaaA2 complex (*c.f.* Fig. 1); lane 2, sample of a washed and redissolved crystal; lane 3, sample of the mother liquor surrounding the crystal. (*d*) Diffraction pattern of a crystal similar in size to that shown in (*b*) and from which the data set reported in Table 1 was collected. It shows diffraction spots up to 3.8 Å resolution (the 3.8 Å resolution limit is indicated by an orange circle). The dashed box displays an enlargement of the diffraction pattern close to the 3.8 Å resolution limit.

complexes have been shown to aptly bind their promoter region to regulate expression of the operon. The findings presented in this paper suggest that, like the VapBC complexes, the *E. coli* O157 ParE2–PaaA2 complex is globular and unique in its stoichiometry and does not form different extended structures as in the cases of CcdAB, Kis–Kid and Phd–Doc. Although the architectural principles of the ParE2–PaaA2 complex resemble those of the VapBC proteins, their oligomerization states are dissimilar: whereas VapBC complexes form heterooctamers, our results suggest that the ParE2–PaaA2 complex is arranged as a heterododecamer. This would make it the largest toxin–antitoxin complex identified to date. The biological function of this entity still remains speculative. *In vivo*, this toxin–antitoxin complex has been shown to partially repress the expression of the *paaR2-paaA2-parE2* operon and to enhance the repression activity of PaaR2 on its own (Hallez *et al.*, 2010). This suggests that the ParE2–PaaA2 complex possesses some DNA-binding activity. Furthermore, it acts in concert with the regulator PaaR2 to ensure proper transcription regulation of the *paaR2-paaA2-parE2* module in *E. coli* O157 (Hallez *et al.*, 2010).

This work was supported by FWO grant G.0090.11N and by grants from OZR-VUB, the Hercules Foundation and VIB. YS and AGP received a predoctoral and a postdoctoral fellowship, respectively, from FWO. TJ is a postdoctoral fellow at the FNRS. LVM thanks the Fonds de la Recherche Scientifique (FRSM-3.4530.04) and the Fonds

Brachet for financial support. The authors thank Andrew Thompson for beamline support.

References

Amitai, S., Kolodkin-Gal, I., Hananya-Meltabashi, M., Sacher, A. & Engelberg-Kulka, H. (2009). *PLoS Genet.* **5**, e1000390.
Bernard, P. & Couturier, M. (1992). *J. Mol. Biol.* **226**, 735–745.
Bertani, G. (1951). *J. Bacteriol.* **62**, 293–300.
Bravo, A., de Torrontegui, G. & Díaz, R. (1987). *Mol. Gen. Genet.* **210**, 101–110.
Brown, B. L., Grigoriu, S., Kim, Y., Arruda, J. M., Davenport, A., Wood, T. K., Peti, W. & Page, R. (2009). *PLoS Pathog.* **5**, e1000706.
Buts, L., Lah, J., Dao-Thi, M.-H., Wyns, L. & Loris, R. (2005). *Trends Biochem. Sci.* **30**, 672–679.
Christensen, S. K., Mikkelsen, M., Pedersen, K. & Gerdes, K. (2001). *Proc. Natl Acad. Sci. USA*, **98**, 14328–14333.
Christensen-Dalsgaard, M. & Gerdes, K. (2008). *Nucleic Acids Res.* **36**, 6472–6481.
Dalton, K. M. & Crosson, S. (2010). *Biochemistry*, **49**, 2205–2215.
Dao-Thi, M.-H., Charlier, D., Loris, R., Maes, D., Messens, J., Wyns, L. & Backmann, J. (2002). *J. Biol. Chem.* **277**, 3733–3742.
Dao-Thi, M.-H., Van Melderen, L., De Genst, E., Afif, H., Buts, L., Wyns, L. & Loris, R. (2005). *J. Mol. Biol.* **348**, 1091–1102.
David, G. & Pérez, J. (2009). *J. Appl. Cryst.* **42**, 892–900.
De Jonge, N., Garcia-Pino, A., Buts, L., Haesaerts, S., Charlier, D., Zangger, K., Wyns, L., De Greve, H. & Loris, R. (2009). *Mol. Cell*, **35**, 154–163.
Dienemann, C., Bøggild, A., Winther, K. S., Gerdes, K. & Brodersen, D. E. (2011). *J. Mol. Biol.* **414**, 713–722.
Fiebig, A., Castro Rojas, C. M., Siegal-Gaskins, D. & Crosson, S. (2010). *Mol. Microbiol.* **77**, 236–251.
Fischer, H., de Oliveira Neto, M., Napolitano, H. B., Polikarpov, I. & Craievich, A. F. (2010). *J. Appl. Cryst.* **43**, 101–109.
Frampton, R., Aggio, R. B., Villas-Bôas, S. G., Arcus, V. L. & Cook, G. M. (2012). *J. Biol. Chem.* **287**, 5340–5356.
Garcia-Pino, A., Balasubramanian, S., Wyns, L., Gazit, E., De Greve, H., Magnuson, R. D., Charlier, D., van Nuland, N. A. & Loris, R. (2010). *Cell*, **142**, 101–111.
Garcia-Pino, A., Christensen-Dalsgaard, M., Wyns, L., Yarmolinsky, M., Magnuson, R. D., Gerdes, K. & Loris, R. (2008). *J. Biol. Chem.* **283**, 30821–30827.
Gerdes, K., Christensen, S. K. & Løbner-Olesen, A. (2005). *Nature Rev. Microbiol.* **3**, 371–382.
Gerdes, K., Rasmussen, P. B. & Molin, S. (1986). *Proc. Natl Acad. Sci. USA*, **83**, 3116–3120.
Hallez, R., Geeraerts, D., Sterckx, Y., Mine, N., Loris, R. & Van Melderen, L. (2010). *Mol. Microbiol.* **76**, 719–732.
Hanahan, D., Jessee, J. & Bloom, F. R. (1991). *Methods Enzymol.* **204**, 63–113.
Hayes, F. & Van Melderen, L. (2011). *Crit. Rev. Biochem. Mol. Biol.* **46**, 386–408.
Jiang, Y., Pogliano, J., Helinski, D. R. & Konieczny, I. (2002). *Mol. Microbiol.* **44**, 971–979.
Kabsch, W. (2010). *Acta Cryst.* D**66**, 125–132.
Kamada, K. & Hanaoka, F. (2005). *Mol. Cell*, **19**, 497–509.
Kamada, K., Hanaoka, F. & Burley, S. K. (2003). *Mol. Cell*, **11**, 875–884.
Kamphuis, M. B., Monti, M. C., van den Heuvel, R. H., Santos-Sierra, S., Folkers, G. E., Lemonnier, M., Díaz-Orejas, R., Heck, A. J. & Boelens, R. (2007). *Proteins*, **67**, 219–231.
Kolodkin-Gal, I., Verdiger, R., Shlosberg-Fedida, A. & Engelberg-Kulka, H. (2009). *PLoS One*, **4**, e6785.
Konarev, P. V., Petoukhov, M. V., Volkov, V. V. & Svergun, D. I. (2006). *J. Appl. Cryst.* **39**, 277–286.
Laemmli, U. K. (1970). *Nature (London)*, **227**, 680–685.
Lehnherr, H., Maguin, E., Jafri, S. & Yarmolinsky, M. B. (1993). *J. Mol. Biol.* **233**, 414–428.
Leplae, R., Geeraerts, D., Hallez, R., Guglielmini, J., Drèze, P. & Van Melderen, L. (2011). *Nucleic Acids Res.* **39**, 5513–5525.
Li, G.-Y., Zhang, Y., Inouye, M. & Ikura, M. (2009). *J. Biol. Chem.* **284**, 14628–14636.
Liu, M., Zhang, Y., Inouye, M. & Woychik, N. A. (2008). *Proc. Natl Acad. Sci. USA*, **105**, 5885–5890.
Magnuson, R. D. (2007). *J. Bacteriol.* **189**, 6089–6092.
Maisonneuve, E., Shakespeare, L. J., Jørgensen, M. G. & Gerdes, K. (2011). *Proc. Natl Acad. Sci. USA*, **108**, 13206–13211.
Maté, M. J., Vincentelli, R., Foos, N., Raoult, D., Cambillau, C. & Ortiz-Lombardía, M. (2012). *Nucleic Acids Res.* **40**, 3245–3258.
Mutschler, H., Gebhardt, M., Shoeman, R. L. & Meinhart, A. (2011). *PLoS Biol.* **9**, e1001033.
Oberer, M., Zangger, K., Gruber, K. & Keller, W. (2007). *Protein Sci.* **16**, 1676–1688.
Ogura, T. & Hiraga, S. (1983). *Proc. Natl Acad. Sci. USA*, **80**, 4784–4788.
Pandey, D. P. & Gerdes, K. (2005). *Nucleic Acids Res.* **33**, 966–976.
Porath, J., Carlsson, J., Olsson, I. & Belfrage, G. (1975). *Nature (London)*, **258**, 598–599.
Studier, F. W., Rosenberg, A. H., Dunn, J. J. & Dubendorff, J. W. (1990). *Methods Enzymol.* **185**, 60–89.
Tan, Q., Awano, N. & Inouye, M. (2010). *Mol. Microbiol.* **79**, 109–118.
Towbin, H., Staehelin, T. & Gordon, J. (1979). *Proc. Natl Acad. Sci. USA*, **76**, 4350–4354.
Tsilibaris, V., Maenhaut-Michel, G., Mine, N. & Van Melderen, L. (2007). *J. Bacteriol.* **189**, 6101–6108.
Uversky, V. N. (1993). *Biochemistry*, **32**, 13288–13298.
Van Melderen, L. (2010). *Curr. Opin. Microbiol.* **13**, 781–785.
Vesper, O., Amitai, S., Belitsky, M., Byrgazov, K., Kaberdina, A. C., Engelberg-Kulka, H. & Moll, I. (2011). *Cell*, **147**, 147–157.
Winn, M. D. *et al.* (2011). *Acta Cryst.* D**67**, 235–242.
Winther, K. S. & Gerdes, K. (2011). *Proc. Natl Acad. Sci. USA*, **108**, 7403–7407.
Winther, K. S. & Gerdes, K. (2012). *Nucleic Acids Res.* doi:10.1093/nar/gks029.
Yamaguchi, Y. & Inouye, M. (2009). *Prog. Mol. Biol. Transl. Sci.* **85**, 467–500.
Yamamoto, S., Kiyokawa, K., Tanaka, K., Moriguchi, K. & Suzuki, K. (2009). *J. Bacteriol.* **191**, 4656–4666.
Yuan, J., Sterckx, Y., Mitchenall, L. A., Maxwell, A., Loris, R. & Waldor, M. K. (2010). *J. Biol. Chem.* **285**, 40397–40408.
Zhang, Y. & Inouye, M. (2011). *Mol. Microbiol.* **79**, 1418–1429.
Zhang, Y., Zhang, J., Hoeflich, K. P., Ikura, M., Qing, G. & Inouye, M. (2003). *Mol. Cell*, **12**, 913–923.